Title

A Modular Array to Detect Complex Fragments Produced in Intermediate-Energy Reverse-Kinematics Reactions

Journal

Nuclear Instruments and Methods in Physics Research A, 311

Authors

Kehoe, W.L.
Mignerey, A.C.
Moroni, A.
et al.

Publication Date

1991-07-01

LBL-31005
Preprint

Lawrence Berkeley Laboratory
UNIVERSITY OF CALIFORNIA

Submitted to Nuclear Instruments and Methods in Physics Research A

A Modular Array to Detect Complex Fragments Produced in Intermediate-Energy Reverse-Kinematics Reactions

W.L. Kehoe, A.C. Mignerey, A. Moroni, I. Iori, G.F. Peaslee, N. Colonna,
K. Hanold, D.R. Bowman, L.G. Moretto, M.A. McMahan,
J.T. Walton, and G.J. Wozniak

July 1991

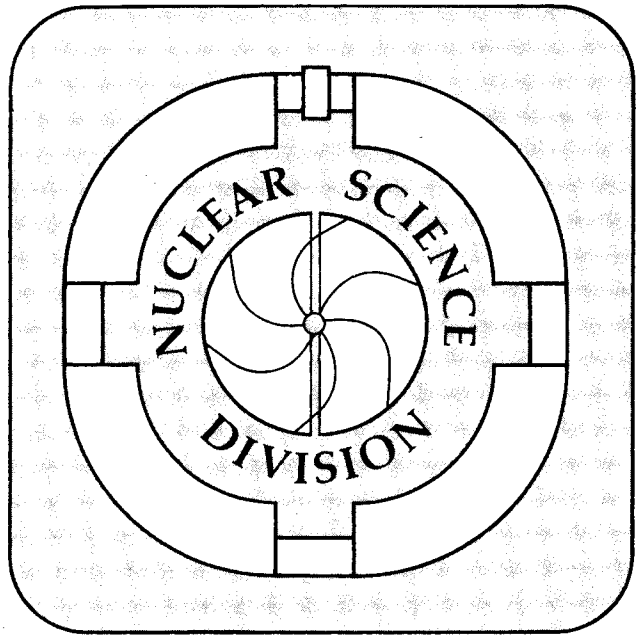

Prepared for the U.S. Department of Energy under Contract Number DE-AC03-76SF00098

DISCLAIMER

DISCLAIMER

LBL-31005

A Modular Array to Detect Complex Fragments Produced in Intermediate-Energy Reverse-Kinematics Reactions

W.L. Kehoe and A.C. Mignerey

Department of Chemistry and Biochemistry
University of Maryland
College Park, MD 20742, USA

A. Moroni and I. Iori

Departmento di Fisica
Universite di Milano and Istituto Nazionale de Fisica Nucleare
Sezione di Milano, Via Celoria 16, 20133, Milano, Italy

G.F. Peaslee, N. Colonna, K. Hanold, D.R. Bowman, L.G. Moretto,
M.A. McMahan, J.T. Walton, and G.J. Wozniak

Nuclear Science Division
Lawrence Berkeley Laboratory
University of California
Berkeley, CA 94720, USA

July 1991

This work was supported by the Director, Office of Energy Research, Division of Nuclear Physics of the Office of High Energy and Nuclear Physics, of the U.S. Department of Energy under Contract Numbers DE-AC03-76SF00098 and DE-FG05-87ER40321.

A MODULAR ARRAY TO DETECT COMPLEX FRAGMENTS PRODUCED IN INTERMEDIATE-ENERGY REVERSE-KINEMATICS REACTIONS

W. L. Kehoe* and A. C. Mignerey

Department of Chemistry and Biochemistry, University of Maryland, College Park, MD 20742, USA

A. Moroni and I. Iori

Departmento di Fisica, Universite di Milano and Istituto Nazionale di Fisica Nucleare, Sezione di Milano, Via Celoria 16, 20133, Milano, Italy

G. F. Peaslee†, N. Colonna, K. Hanold, D. R. Bowman†, L. G. Moretto, M. A. McMahan, J. T. Walton, and G. J. Wozniak

Nuclear Science Division, Lawrence Berkeley Laboratory, 1 Cyclotron Road, Berkeley, CA 94720, USA

Abstract

A segmented silicon-silicon-plastic array was constructed for studying complex fragment production in heavy-ion reactions with incident energies of 35 - 100 MeV/u. The array was designed: 1) to measure the energy, position and charge of fragments with $1 \leq Z \leq Z_{proj}$; 2) to have high efficiency for detecting fragments produced in reverse-kinematics reactions; 3) to detect events with two or more fragments; and 4) to have a flexible configuration. Each array telescope consists of a 300-μm Si detector, a 5-mm Si(Li) detector and a 7.6-cm plastic scintillator. The elements of the telescope are held by interconnecting modular packages which allow the telescopes to be close packed about the beam direction. This modular array has been used in several different experimental configurations and examples of its performance are presented.

* Present address: Laboratory of Nuclear Science, 26-402, Massachusetts Institute of Technology, 77 Massachusetts Ave, Cambridge, MA 02139, USA.

† Present address: National Superconducting Cyclotron Laboratory, Michigan State University, East Lansing, MI 48824, USA.

1. Introduction

At low bombarding energies (10 MeV/u), heavy-ion reactions lead on the one hand to the formation of compound nuclei, which in turn can decay by evaporating neutrons, light-charged particles and fissioning, or, on the other hand, to deep-inelastic products. Because of the predominantly binary character of these reactions and the limited range in mass and energy of the reaction products, their study does not usually require extensive solid angle coverage or sophisticated detection systems.

At higher bombarding energies, fragments intermediate in mass between light-charged particles and evaporation residues are copiously produced. The rapid rise in the production of these fragments, usually referred to as complex fragments or intermediate mass fragments, has stimulated great theoretical [1-3] and experimental interest [4-7]. In particular, multifragment processes are currently under intense investigation since they could disclose information on the behavior of nuclear matter under extreme conditions of density and temperature.

From the experimental standpoint, the characterization of multifragment decays of highly excited nuclear systems requires the simultaneous detection and identification of numerous and vastly different fragments over the entire emission phase space. Only in this way can essential information be extracted and unbiased kinematical reconstructions of the events be attempted. The need for studying multifragment decays of highly excited nuclear systems has led in the past years to the construction of several 4π detection systems[8 - 13]. Near complete coverage of the solid angle and good granularity are some of the characteristics that make these systems useful tools for the investigation of normal-kinematics heavy-ion reactions. However, the high fabrication costs, voluminous dimensions, complicated data processing and acquisition systems, and typically high thresholds may constitute serious limitations to the use of these systems.

An alternative approach is to utilize reverse-kinematics reactions[14] (heavy projectile impinging on a light target) to study the multifragment decay properties of hot nuclei[6,7,15-18]. For this class of reactions, the center-of-mass velocity is usually large enough for the reaction products to be confined to forward angles in the laboratory system, and efficient coverage of the

emission phase space can be achieved with a modest sized detection system. Furthermore, the strong kinematical boost in the laboratory makes the detection and identification of complex fragments an easier task. Finally, threshold problems that often limit the detection and identification of low energy target-like fragments in normal-kinematics reactions are less restrictive in reverse-kinematics reactions, due to the forward boost in the laboratory frame.

In order to study complex-fragment emission mechanisms by exploiting features of reverse-kinematics reactions with incident energies of 35 - 100 MeV/u, a close-packed array of silicon(Si)-silicon(Si)-plastic(Pl) telescopes has been built. This paper will discuss its design, fabrication and performance. In Section 2 the design and fabrication of the telescope components [15] and of the array mounts are presented, together with examples of the experimental configurations. The performance of the Si-Si-Pl Array telescopes is described in Section 3.

2. Si-Si-Pl Array Design

2.1. Design Goals

The design of this array exploits the forward-focusing characteristics of reverse-kinematics reactions to build a modest-sized detection system with a large coverage of the emission phase space to study complex-fragment production mechanisms. If the projectile is substantially heavier than the target, the reaction products are strongly forward focused in the laboratory system. In fig. 1 a schematic diagram of the binary decay of a compound nucleus in a reverse-kinematics reaction is shown. For sequential multifragment emission, it can be shown that all of the fragments of a given mass lie inside the cone described by the binary decay. By placing detectors at forward angles, a large fraction of the emission cone can be covered. With the present array, the coverage is most efficient for intermediate mass fragments. Due to their smaller emission velocities, fragments similar in mass to the projectile are focused very close to the beam direction, where it is very difficult to place detectors. On the other hand, due to their large emission velocities, protons and

alpha particles have the largest angular range in the laboratory, and the forward array will typically detect only a small fraction of the light charged particles emitted in these reactions.

Three design criteria were established for this detection system. First, in order to measure the energy, position and charge of reaction products from protons up to the projectile charge (e.g. La, Z = 57), a large dynamic range is required. Second, to study the transition from binary decay to multibody decay, sufficient segmentation and solid angle coverage is needed in order to detect several complex fragments in coincidence. Finally, the array should have a flexible design, capable of adjusting to changes in the reaction kinematics in order to optimize the detection efficiency.

To identify all charged particles with $Z \geq 1$, over a large energy range, a three element telescope was chosen. Each telescope consists of a 300-μm and a 5-mm silicon detector followed by a 7.6-cm plastic scintillator. The three detectors are employed in two successive ΔE-E telescopes with the 5-mm detector common to both telescopes. The first and second detectors are used to identify fragments with $Z \geq 4$, and the second and third detectors to identify fragments with $Z < 4$. Because of the very large range of energy deposited in the 5-mm detector, two different gains are usually employed: a low gain for ions that stop in the silicon detector and a high gain for ions that pass through to the plastic detector.

In meeting our first design criterion, silicon detectors offer important advantages over gas or scintillation detectors. They have better energy and charge resolution and a more linear response, over a wide range of energies that is nearly independent of the charge of the detected particles. In addition, they have a high stopping power (dE/dx) for heavy ions. The energy range of ions which stop in a 5-mm silicon detector is shown in fig. 2, where the ranges[19], in silicon of representative ions from helium through xenon, are plotted as a function of energy. The horizontal lines correspond to the thicknesses the 300-μm Si and 5-mm Si(Li) detectors used in the array. Heavy-ions ($Z < 54$) with >25 MeV/u punch through the 300-μm detector, while ions with $Z > 16$ and ≤100 MeV/u will stop in the 5-mm detector. The relatively high energy threshold of the 300-

μm Si detector is only a minor drawback in reverse-kinematics reactions, since most of the reaction products are emitted with nearly beam velocity.

Our second design goal of measuring the transition from two-body to multi-body decay requires that the array have sufficient granularity and efficiency to detect several fragments in coincidence. The previously mentioned characteristics of reverse-kinematics reactions allowed for the design of a segmented array of modest size with each modular telescope roughly 5 x 5 cm^2 in cross sectional area.

To achieve our third design goal of a flexible configuration, a modular telescope design was chosen. Most 4π detector arrays are designed for normal kinematics where the reaction kinematics vary slowly with the bombarding energy. In such arrays the detector elements, whose shapes are usually truncated polyhedrons [8-12], can be designed to be placed at a fixed distance from the target. In reverse kinematics the reaction kinematics change rapidly with bombarding energy and it is necessary to adjust the detector configuration. The mount was constructed so that the array could be positioned at different distances from the target with the front face of each telescope normal to the target.

2.2. Detector Specifications and Fabrication

Two types of silicon detectors are used in each array telescope[20]. The 300-μm device is an oxide passivated diffused junction n^+p diode fabricated from 5000 Ω-cm p-type silicon. The 5-mm device is a lithium-drifted silicon diode, Si(Li), fabricated from 1000 Ω-cm p-type silicon. Both of these devices were fabricated by the Silicon Detector Laboratory at Lawrence Berkeley Laboratory (LBL). Diffused-junction silicon detectors are made by diffusing an n-type impurity into the p-type material under high temperature conditions[21]. This procedure produces thin, rugged and stable detectors. Lithium-drifted silicon detectors are produced by diffusing lithium onto the surface of a p-type silicon crystal, and drifting it through the device to form a compensated region[22]. This produces thick detectors capable of stopping fragments with relatively high energy. For both devices a square geometry was chosen to facilitate close packing of adjacent

telescopes. Better packing could be achieved with silicon detectors having more complicated shapes. However, larger costs were anticipated to make these more complex devices.

The front faces of the silicon detectors are 50.8 x 50.8 mm^2 squares, and have active areas of 44.8 x 44.8 mm^2. A plan view of the device with the dimensions and their allowed tolerances is shown in fig. 3. The size of the active area was set by the commercial availability of 3-inch diameter silicon crystals and the fabrication requirement that the lithium-drifted devices have a dead area of at least 3 mm around the edge of the device. The 300-μm Si detectors were made from 3-in diameter wafers with a thickness of 381 ± 10 μm, and etched in stages to an average thickness of about 290 μm. The thickness nonuniformity of these devices ranged from 2 - 10%. The 5-mm Si(Li) detectors were cut from 3-in diameter material, and lapped to have an average thickness of 4.88 ± 0.07 mm. The thickness nonuniformity of these devices is ±50 μm (≤2%). Total entrance window thicknesses were typically 1 μm and 25 μm for the 300-μm and 5-mm detectors, respectively.

Both types of silicon detectors are position sensitive in one dimension and provide position information using the method of resistive charge division. In this method, the position signal (XΔE or YE) is equal to the deposited energy (E) of the incident particle multiplied by the ratio of the distances between the ground contact and the point of incidence (ΔL) and the total length of the resistive layer (L); that is,

$$YE = E\frac{\Delta L}{L}. \qquad (1)$$

In a telescope, the position-sensitive dimensions of the 300-μm and the 5-mm silicon detectors are oriented 90° relative to each other to determine the X- and Y-position of the charged particles traversing the telescope.

Calibration of position-sensitive detectors having a continuous resistive layer is typically performed by placing a position mask in front of each detector. However, this procedure is cumbersome, greatly decreases the counting rate and requires separate calibration runs. With the

Si-Si-Pl Array, position calibrations of the telescopes are unnecessary because the silicon detectors are self-calibrating. This is accomplished by creating a resistor chain across the front face of the device using strips of low resistivity material separated by gaps of high resistivity material. In such devices, the ratio of the position and energy signals has discrete levels. The dimensions of the strips and gaps are determined by two factors: (1) the number of strips necessary for good position resolution based on the typical size and divergence of the LBL Bevalac's beam spot, and (2) the gap size needed to achieve a resistance of 100 Ω between each strip on the 300-μm Si detector; this value was experimentally determined to give optimal peak-to-valley separation of the peaks in the position spectrum.

The active area of each type of device is divided into 15 strips of 2.42 mm, and 14 gaps of 0.607 mm, as shown in fig. 3. The strips on the 300-μm Si detectors are implanted using 25-keV boron ions. The low resistivity strips have a boron concentration of ~2 x 10^{14} atoms/cm^2, whereas the high resistivity gaps have a lower concentration of ~3 x 10^{13} atoms/cm^2. The resistor chains are produced on the 5-mm Si(Li) detectors by evaporating a very thin layer of palladium over the entire device, and then evaporating gold strips on top of the palladium layer. Two gold position contacts are evaporated parallel to the position strips along the front edges of each device. The back of the 5-mm Si(Li) device was evaporated with gold to make the energy signal contact; a small square of aluminum was evaporated on the back of the 300-μm Si device to make its energy signal contact.

The very thin palladium (Pd) resistive layers are difficult to produce and the resistance values sometimes change with time. More recently, an alternative fabrication technique has been utilized that produces more stable resistances. In this technique, the resistive division is achieved by laying down two strips of Pd, perpendicular to the gold strips. Because the thin Pd strips can be much thicker than the Pd sheet and still produce the same resistance, better uniformity of the resistance is achieved.

The Bicron BC-400[23] plastic scintillator used in the array telescope is a common type of plastic scintillator. It has a high light output (65% of anthracene), good light transmission

properties and a decay time of 2.4 ns. Each scintillator detector has a simple rectangular geometry. The entrance window is 52.1 x 52.1 mm^2 and the length is 76.2 mm. The dimensions of the complete detector, including light-tight epoxy paint around the detector, light guide, photomultiplier tube and base, are 53.0 x 53.0 x 280 mm^3. The entrance window of the detector is made light tight by evaporating a very thin layer (2.5 μm) of aluminum on it, and is polished to a mirror finish. The window thickness is kept as thin as possible to minimize the energy loss of particles entering the detector. An RCA model 2060 photomultiplier tube (PMT) [24] with a ten stage dynode is coupled to the plastic by a Lucite light guide. The PMT and base are covered by a mu-metal shield having a diameter of 45 mm.

2.3 Array Telescope Design

Three connecting modular elements, each containing one detector, compose an array telescope. Each detector is mounted in a self-contained package fabricated with pieces of Nema G10. This material was used for the detector packaging because it is strong, a good insulator, and available with copper cladding which allows for electrical contacts. The front face of each package is 55.0 x 57.0 mm^2, and the active area is 64% of the total area of each telescope.

The individual components that make up a telescope are shown in an exploded view in fig. 4. In front-to-back order: frame A holds a gold foil deposited on a thin sheet of polypropylene which is used to suppress low-energy electrons and x-rays. Frames B, C, Teflon A and frame D compose the package for the 300-μm Si detector. The detector fits inside frame C, and Teflon A acts as an insulator and spacer. The frames are held together by four screws located at the corners of the package. The 5-mm Si(Li) detector package is of a similar design. It is composed of frames E, F, Teflon B and frame G, with the detector fitting inside frame F. The package for the plastic detector is a rectangular cavity formed by pieces of G10 glued together, which have copper cladding on the exterior only, and are connected to an aluminum back plate. This package was designed to slide over the PMT, to completely cover the sides and back of the plastic detector, and to be secured to the PMT using set screws in the back plate.

A key feature in the design of the detector packages that allows for close packing of the telescopes is the use of small pin and socket connectors [25] to carry the signal from one modular element to the next. These connectors use a twist pin contact that compresses when the pins are connected, which provides electrical contact, alignment and mechanical support of the detector packages. Each modular element has eight connectors, four on each 55-mm side. The connectors provide an isolated path through the telescope for the six signals: two X-position signals and an energy signal for the 300-μm Si detector, two Y-position signals and an energy signal for the 5-mm Si(Li) detector, and two additional connectors which carry no signal and are available as spare signal lines. For each detector, one of the two position signals is terminated to 50 Ω. Fig. 5 is a photograph of the three detectors elements and their associated packaging.

2.4 Array Mount Design

The mount for the array was designed to arc in both the horizontal (X) and vertical (Y) directions. This allows the rectangular faces of the array telescopes to move on a surface of a sphere by adjusting horizontal and vertical arcs on the mount to the proper opening angle, determined by the distance of the array from the target. Fig. 6 is a front elevation of a 3 x 3 configuration showing the geometrical difference between a flat wall (a), where the sides of the telescope packages touch flush against each other, and squares on a sphere (b), where only the corners of the outermost telescope packages touch. By adjusting the arcs of the mount, the centers of each telescope are kept normal to the target. In this way, only small corrections are needed to convert the internal coordinates X and Y to the spherical coordinates θ_{lab} (in-plane angle) and φ_{lab} (out-of-plane angle). By designing the array to be placed at different distances from the target, a small loss of active area results with a corresponding decrease in the coincidence efficiency. Gaps between the telescopes develop as the array opens, becoming widest when the array is closest to the target (d = 35 cm). At distances greater than 3 m from the target, the mount can collapse on itself to form a wall, since the opening angle is less than 1°.

Because the detected fragments have a large range of energy and mass, it is useful to calibrate each telescope with a number of calibration beams of different energies and masses. At intermediate energies the grazing angles are very small (<5°) and elastic scattering reaches only the most forward telescopes. To facilitate the calibration of the energy response of the detectors, motor-driven mechanical mounts were built to provide motion in both the horizontal and vertical directions. To map out the response and to measure the non-uniformity of the ΔE detectors as a function of the X and Y positions, each telescope is positioned in the beam direction and exposed to several calibration beams. Typically, each detector is moved slowly across the beam. By calibrating the telescopes as a function of position and correcting for nonuniformities, significantly improved particle identification can be achieved.

Initially, the silicon detectors were operated in vacuum without cooling. However, it was observed that the leakage currents increased with time after evacuating the scattering chamber and recovered after letting up to atmospheric pressure. This behavior was attributed to the heating of the silicon detectors by the PMTs in vacuum and their subsequent cooling in atmosphere. Since silicon detectors have better performance characteristics when cooled and because radiation damage is suppressed, a cooling system was installed. Cooling lines are attached from an alcohol refrigerator to the outside of the telescope mount, as it is difficult to cool the detectors directly, due to the close-packed mount. Even with poor thermal contact to the detectors, the detector temperatures are reduced with a corresponding reduction of the detector leakage currents. With the cooling on and applied voltages of 700 V and 100 V, the leakage currents of the E and ΔE detectors are typically less than 5 μA and 1 μA, respectively.

2.5 *Electronics*

Because of their large areas, the thin ΔE detectors have large capacitances and slow risetimes (t_r ~200 ns). The very thick 5-mm detectors have even slower risetimes (t_r ~ 500 ns). Such slow risetimes require long shaping times to insure that all of the charge from an event is collected. In addition, the substantial resistive layer on the detector causes the signal risetime to vary with

position across the device. Furthermore, the collection time varies with the ranges of the fragments in the detector [26]. To maintain a linear response for fragments over a very large Z range, a 4-μs peaking time is used for the linear shaping amplifiers.

A typical electronics scheme for the Si-Si-Pl Array is shown in fig. 7. An event trigger is generated by a coincidence ($\Delta t \sim 500$ns) between the 300-μm Si and the 5-mm Si(Li) detector of any of the array telescopes. The timing of the telescopes is limited by the 5-mm detectors, whose signals have both a poor risetime and a position dependence. Each detector that fires sets a bit in a bit register and stops a time-to-digital converter (TDC). Light-charged particles ($Z \leq 3$) are not taken unless accompanied by a heavier fragment. Constant fraction discriminators on the ΔE detectors are set to exclude particles with $Z < 3$). Energy signals from the two silicon detectors of each telescope are sent to peak-sensitive analog-to-digital converters (ADC's).

To identify a light-charged particle that punches through to the plastic detector, this signal is sent to a charge-to-digital converter (QDC). In addition, a high-gain signal from each silicon detector is sent to a peak-sensitive ADC. The high-gain signals are obtained by post amplifying the linear output of the shaping amplifier by an additional factor of 10 to 40. Because of the high count rates in the plastic detectors, a fast clear is employed to reject events that only trigger a plastic detector.

When a valid-event trigger is received, the ADC's and TDC's corresponding to the channels with set bits are read out. The event trigger is vetoed by the computer deadtime. The data are processed by a VME data acquisition system and written event-by-event on magnetic tape and to disk for on-line monitoring by a dedicated computer.

2.6 Experimental Configurations

Several configurations of the Si-Si-Pl Array have been used in experiments performed to date. In each configuration the mount for the array was adjusted to the kinematics of the reactions studied, and to conform to the scattering chamber in which the experiment was performed. In figs. 8 & 9 two examples of array configurations used are shown.

To study lower energy reverse kinematic reactions, where the reaction products have a larger relative transverse velocity component, two 3x3 arrays were placed to either side of the beam (see fig. 8) to obtain greater angular coverage [6]. In a second configuration, two 3x3 arrays were placed one behind the other (see fig. 9), the array farthest from the target subtends the central opening in the closer array. This latter configuration was used to study ^{238}U-, ^{197}Au-, and ^{129}Xe-induced reactions at 50 MeV/u [16,18]. The advantage of this array configuration is that even the very heavy reaction products which are emitted at small angles with near beam velocities can be detected. In this same configuration, Si-Si-Pl Array was most recently used as a forward angle array together with the MSU Miniball [12] to give complete 4π coverage.

For some experiments at higher energy, a second 5-mm Si(Li) detector was added to each array telescope in order to stop particles of higher energy in the silicon detectors, which have a more linear response than the plastic detector. This was accomplished by taking advantage of the two unused pin and socket connectors in the modular detector elements. In a 3x4 configuration these telescopes were used to study reactions with beams of 80- and 100-MeV/u ^{139}La on ^{12}C and ^{27}Al [17].

3. Detector Performance

In this section results from various ^{129}Xe- and ^{139}La-induced reactions will be used to illustrate the calibration techniques and the performance of the telescopes.

3.1 Position Calibration and Resolution

As mentioned earlier, the silicon detectors are self calibrating in position by design, and no special runs are required for calibration. In fig 10, the 15 strips of a 5-mm Si(Li) detector are clearly resolved in a density plot of the position (YE) signal plotted as a function of the energy (E) signal. The lowest line corresponds to the strip farthest away from the signal contact.

The position linearization is performed using a method outlined by Kaufman [27]. The distance Y from the grounded end of the detector is given by:

$$Y = (YE - P_0)/(E - E_0)$$

where P_0 and E_0 are related to, but not necessarily equal to, the electronic base-line offsets. Their values are chosen to eliminate any dependence of Y on the energy. In fig. 11 a typical spectrum of the corrected position is displayed for an optimal choice of P_0 and E_0, demonstrating the good position resolution of these detectors.

3.2 Energy Calibration and Resolution

The energy calibrations are obtained by directly exposing the 300-μm Si and 5-mm Si(Li) detectors to low intensity single or multiple calibration beams with masses between A = 12 and 139. In addition, p, d and α-particle beams are utilized to calibrate the plastic scintillators. The intensity of the calibration beams is adjusted to <100 particles/sec so as to minimize the radiation damage to the silicon detectors. By using multiple beams, an extensive energy calibration of the silicon detectors could be performed in a relatively short amount of beam time. To perform the equivalent energy calibration with individual beams, the calibration time would exceed the data taking time.

The Bevalac, which consists of the coupled SuperHILAC and Bevatron accelerators, can accelerate multiple-ion species having the same charge-to-mass ratio[28]. An example of a multiple calibration beam (45-MeV/u $^{14}N^{4+}$, $^{28}Si^{8+}$, $^{56}Fe^{16+}$ and $^{84}Kr^{24+}$) produced at the Bevalac is shown in fig. 12. This quadruplet beam consists of four ions having a charge-to-mass ratio of 2/7. To produce a quadruplet beam, the charge-to-mass ratio of all four ions is kept the same at all stages of the acceleration from the ion source through the SuperHILAC and the Bevatron. Ions with a charge-to-mass ratio of 1/14 ($^{14}N^{1+}$, $^{28}Si^{2+}$, $^{56}Fe^{4+}$ and $^{84}Kr^{6+}$) are produced in the ion source by introducing nitrogen and krypton as gases, while the iron and silicon are introduced from an iron sputter electrode with a silicon insert. Ions with a charge-to-mass ratio of 1/14 are first accelerated through the prestripper of the SuperHILAC, where they are stripped up to a

charge-to-mass ratio of 2/7. These ions are further accelerated through the poststripper to 5 MeV/u and injected into the Bevatron, where they are accelerated to 45 MeV/u.

To expose all of the detectors to a calibration beam, the in-plane telescopes are swept across the beam, then the array is raised or lowered remotely and the out-of-plane telescopes are then swept through the beam. The 5-mm Si(Li) detectors are calibrated without the 300-μm Si detectors in front. The measured energy in the 5-mm Si(Li) detectors, with and without the 300-μm detectors in front, is then used to calibrate the 300-μm Si detectors. Finally, the 5-mm detectors are removed and the plastic detectors are calibrated with α-particle and other light ion beams.

Corrections are made for the pulse-height defect in the 5-mm Si(Li) detectors using the systematics of Moulton et al.[29], in which a simple power-law formula is derived to calculate the energy loss due to the pulse-height defect as a function of the measured energy and charge of the ion. No correction for the pulse-height defect is made for the 300-μm Si detector, because the identified particles do not stop in this detector. Corrections for energy losses in the target and the Au-absorber foils in front of telescopes are made using range energy tables[19]. An energy resolution of 1 % is easily achieved over a very broad dynamic range.

3.3 Particle Identification

For a ΔE-E telescope a plot of the energy lost in the transmission detector versus the energy deposited in the stopping detector gives an intensity pattern of alternating valleys and ridges (see fig. 13), where each ridge corresponds to fragments with a different atomic number (Z). The large dynamic range of the silicon telescope allows the identification of the Z ridges for all atomic numbers up to the projectile (Z = 54) in this case. By applying a suitable identification algorithm, the charge of the detected fragment is extracted from the measured E and ΔE signals. An example of the charge spectrum from one telescope is shown in fig. 14. Each peak corresponds to a different element. After correcting for nonuniformities in the thickness of the ΔE detector, excellent Z resolution is obtained as can be seen from fig. 14 where individual elements are resolved over the entire range of the detected fragments.

By utilizing the high gain signal from the 5-mm detector and the plastic signal, ΔE-E contour plots are constructed. Light fragments that punch through the 5-mm detector and stop in the plastic detector are also identified. In fig. 15 isotopic resolution is observed for hydrogen, helium and lithium isotopes. For Z = 1, three strong lines corresponding to p, d and t are seen with a substantial number of high energy events (> 100 MeV/u) which punch through the 7.6 cm plastic detector. A very strong ^{4}He line is observed along with weaker ^{3}He and ^{6}He lines. Weak ^{6}Li, ^{7}Li and ^{8}Li lines are also observed, as well as a few high-energy beryllium isotopes in the upper right hand corner of fig. 15.

3.4 *Coincidence events*

The Si-Si-Pl Array has been used to study binary and multi-body decays of hot nuclear systems formed in a number of reverse-kinematics reactions. For 40-MeV/u ^{139}La-induced reactions on four targets, the total charge detected in the array is plotted in fig. 16 for 2-, 3- and 4-fold coincidence events. The very asymmetric ^{139}La + ^{12}C reaction forms a warm nuclear system with very little missing charge, presumably in the form of evaporated light charged particles. These data show that this warm system decays into two or three large fragments, which contain a very large fraction of the total charge present in the entrance channel ($Z_{entrance}$ = 63). For the hotter ^{139}La + ^{27}Al system, more charged particles are emitted and a smaller fraction of the entrance-channel charge is contained in these 2-, 3- and 4- fragment events. For the very hot ^{139}La + ^{51}V, ^{nat}Cu systems, only about 50% of the entrance-channel charge is measured when four fragments are detected. These very hot systems emit several complex fragments and a large number of light charged particles for which the array is not very efficient.

5. Summary

In this paper we have discussed the design, fabrication and performance of a Silicon-Silicon-Plastic Array for the detection of complex fragments produced in intermediate-energy reverse-kinematics reactions. The three-element telescopes have a large dynamic range and are capable of detecting with good position, energy and charge resolution, a large range of fragments, from light charged particles up to $Z \sim 55$. The modular design of the array telescopes and the adjustable two-dimensional mount for the array have proven to be flexible and adaptable. This array has been utilized to study several reaction systems. Examples of both binary and multi-body decays of hot nuclear systems observed with this array have been presented.

Acknowledgements

The authors would like to acknowledge the elegant mechanical design work of Don Malone and Luigi Dellerro; the fine craftsmanship and dedication of John Anderson, Angelo Cortesi, Warren Harnden and Heinrich Sommer; and the excellent electronics support of Don Landis and Norm Madden, all of which were essential for the success of this project. This work was supported by the Director, Office of Energy Research, Division of Nuclear Physics of the Office of High Energy and Nuclear Physics of the US Department of Energy under Contracts DE-AC03-76SF00098 and DE-FG05-87ER40321.

References

[1] J. B. Bondorf, R. Donangelo, I. N. Mishustin and H. Schulz, *Nucl. Phys.* **A444** (1985) 460.

[2] D. H. E. Gross, Yu-ming Zheng and H. Massman, *Phys. Lett.*. B **200** (1987) 397.

[3] L. G. Moretto, *Nucl. Phys.* **A247**, 21 (1975).

[4] Y. D. Kim, M. B. Tsang, C. K. Gelbke, W. G. Lynch, N. Carlin, Z. Chen, R. Fox, W. G. Gong, R. Mukarami, T. K. Nayak, R. M. Ronningen, H. M. Xu, F. Zhu, and W. Bauer, *Phys. Rev. Lett.* **63**, (1989) 494.

[5] R. Trockel, K. D. Hildenbrand, U. Lynen, W. F. J. Muller, H. J. Rabe, H. Sann, H. Stelzer, W. Trautmann, R. Wada, E. Eckert, P. Krentz, A. Kuhlmichel, J. Pochodzalla and D. Pelte, *Phys. Rev.* C **39**, (1989) 729.

[6] Y. Blumenfeld, N. Colonna, P. Roussel-Chomaz, D. N. Delis, K. Hanold, J. C. Meng, G. F. Peaslee, Q. C. Sui, G. J. Wozniak, and L. G. Moretto, *Phys. Rev. Lett.*, 66 (1991) 576.

[7] L. G. Moretto and G. J. Wozniak, *Prog. Part. Nucl. Phys.* **21**, (1988) 401.

[8] A. Baden, H. H. Gutbrod, H. Löhner, M. R. Maier, A. M. Pozkanzer, T. Renner, H. Riedesel, H. G. Ritter, H. Spieler, A. Warwick, F. Weik, and H. Wieman, *Nucl. Instr. and Meth.* **A203**, (1982) 189.

[9] G. D. Westfall, J. E. Yurkon, J. van der Plicht, Z. M. Koening, B. V. Jacak, R. Fox, G. M. Crawley, M. R. Maier, B. E. Hasselquist, R. S. Tickle, and D. Horn, *Nucl. Instr. and Meth.* **A238**, (1985) 347.

[10] D. G. Sarantites, L. G. Sobotka, T. M. Semkow, V. Abenante, J. Elson, J. T. Hood, Z. Li, N. G. Nicolis, D. W. Stracener, J. Valdes, and D. C. Henley, *Nucl. Instr. and Meth.* **A264**, (1988) 319.

[11] M. M Fowler, T. C. Sangster, M. L. Begemann-Blaich, T. Blaich, J. A. Boissevain, H. C. Britt, Y. D. Chan, A Dacal, D. J. Fields, Z. Fraenkel, A. Gavron, A. Harmon, B. V. Jacak, R. G. Lanier, P. S. Lysaght, G. Mamane, D. J. Massoletti, M. N. Namboodiri, J. Poilot, R. G. Stokstad, M. L. Webb, and J. B. Wilhelmy, *Nucl. Instr. and Meth.* **A281**, (1989) 517.

[12] R. T. de Souza, N. Carlin, Y. D. Kim, J. Ottarson, L. Phair, D. R. Bowman, C. K. Gelbke, W. G. Gong, W. G. Lynch, R. A. Pelak, T. Peterson, G. Poggi, M. B. Tsang and H. M. Xu, *Nucl. Instr and Meth.* **A295** (1990) 109.

[13] J. Galin, X. M. Wang, E. Crema, D. Guerreau, D. X. Jiang, M. Morjean, J. Pouthas, F. Saint-Laurent, A. Sokolov, B. Gatty, D. Jacquet, B. Lott, U. Janke, E. Schwinn, E.

Piasecki, and J. L. Charvet, Proceedings of the 2nd IN2P3-Riken Symposium on Heavy Ion Collisions, Obernai, France, April 9 - 12, 1990, ed. by B. Heusch and M. Ishihara, World Scientific, p. 102.

[14] R. J. Charity, M. A. McMahan, D. R. Bowman, Z. H. Liu, R. J. McDonald, G. J. Wozniak, L. G. Moretto, S. Bradley, W. L. Kehoe, A. C. Mignerey, and M. N. Namboodiri, Phys. Lett. Rev. **56** 1354 (1986).

[15] W. L. Kehoe, University of Maryland, College Park, Ph.D. thesis, October 1989.

[16] G.F. Peaslee, L. G. Moretto, and G. J. Wozniak, Lawrence Berkeley Laboratory preprint, LBL-29014.

[17] D. R. Bowman, G. F. Peaslee, N. Colonna, R. J. Charity, M. A. McMahan, D. Delis, H. Han, K. Jing, G. J. Wozniak, L. G. Moretto, W. L. Kehoe, B. Libby, A. C. Mignerey, A. Moroni, A. Angius, I. Iori, A. Pantaleo, and G. Guarino, *Nucl. Phys.* **A523** (1991) 386.

[18] D. R. Bowman, G. F. Peaslee, R. T. de Souza, N. Carlin, C. K. Gelbke, W. G. Gong, Y. D. Kim, M. A. Lisa, W. G. Lynch, L. Phair, M. B. Tsang, C. Williams, N. Colonna, K. Hanold, M. A. McMahan, G. J. Wozniak, L. G. Moretto, and W. A. Friedman, MSU preprint, MSU-779 (1991).

[19] F. Hubert, A. Fleury, R. Bimbot, and D. Gardès, *Supp. Ann. Phys. Fr.* **5**, (1980) 1.

[20] J. T. Walton, H. A. Sommer, G. J. Wozniak, G. F. Peaslee, D. R. Bowman, W. L. Kehoe, and A. Moroni, IEEE Trans. Nucl. Sci. **37** (1990) 1578.

[21] J. T. Walton and F. S. Goulding, *IEEE Trans. Nucl. Sci.* **NS-34** (1987) 396.

[22] J. T. Walton, H. A. Sommer, D. E. Greiner, and F. S. Bieser, *IEEE Trans. Nucl. Sci.* **NS-25** (1978) 391.

[23] Bicron Corporation, 12345 Kinsman Road, Newbury, Ohio 44065.

[24] RCA Corp., New Holland Ave, Lancaster, PA 17604.

[25] Centi line connectors, ITT, 2107 N. First Street, Suite 440, San Jose, CA 95131.

[26] Glenn F. Knoll, Radiaton Detection and Measurement, John Wiley & Sons, New York, (1979) p. 473.

[27] S. B. Kaufman, B. D. Wikins, M. J. Fluss, and E. P. Steinberg, *Nucl. Instr. and Meth.* **82**, (1970) 117.

[28] G. J. Wozniak et al., to be published.

[29] J. B. Moulton, J. E. Stephenon, R. P. Schmitt, and G. J. Wozniak, *Nucl. Instr. and Meth.* **157**, (1978) 325.

Figure Captions

Fig. 1 Schematic diagram of a reverse kinematics reaction. When the source velocity V_s is larger than the emission velocity V_e, the decay products are strongly focused in the laboratory system. An example is shown where two fragments (A & B) are emitted both forward and backward in the center-of-mass system and are detected at the same laboratory angle θ.

Fig. 2 Range of selected heavy ions in silicon as a function of particle energy. The horizontal lines show the thickness of the 300-μm Si and 5-mm Si(Li) detectors.

Fig. 3 Plan view of the position strips on the front face of the 300-μm Si and 5-mm Si(Li) devices used in the Si-Si-Pl array. Each device has 15 strips 2.42 mm wide and 44.80 mm long. Between the strips are 14 gaps, each 0.607 mm wide.

Fig. 4 Exploded view of the Si-Si-Pl Array telescope showing the components of the detector packages.

Fig. 5 Photograph of the three detector elements which make up a telescope.

Fig. 6 Comparison of two geometries for the front face of a 3 x 3 array: (a) flat wall geometry, and (b) squares on a sphere geometry.

Fig. 7 A schematic electronics diagram for the Si-Si-Plastic Array.

Fig. 8 Two adjacent 3 x 3 Si-Si-Pl arrays. Typically, the beam passes between the left and right secions of the array. However, for this photograph, the array is no longer centered about the beam axis.

Fig. 9 Two 3x3 Si-Si-Pl arrays positioned about the beam. The beam passes through the central position in each array.

Fig. 10 For the 40-MeV/u $^{139}La + ^{40}Ca$ reaction, a density plot is shown of the raw position (YE) signal plotted as a function of the energy (E) signal from a 5-mm Si(Li) detector. The 15 strips of the 5-mm Si(Li) detector are well separated.

Fig. 11 For the 40-MeV/u $^{139}La + ^{40}Ca$ reaction, the calibrated Y position is shown for one of the 5-mm detector. Each peak corresponds to a different strip on the detector. The position is expressed as the distance, in mm, from the grounded edge of the detector.

Fig. 12 Energy spectrum of a 5-mm silicon detector exposed to a quadruplet beam of $^{14}N^{4+}$, $^{28}Si^{8+}$, $^{56}Fe^{16+}$ and $^{84}Kr^{24+}$ from the Bevalac. These four calibration beams have the same charge-to-mass ratio (Q/A = 2/7) and were simultaneously accelerated to 45 MeV/u.

Fig. 13 For the 50-MeV/u $^{129}Xe + ^{nat}Cu$ reaction, the density plot of ΔE vs E clearly shows the ridge lines corresponding to different elements.

Fig. 14 For the 50-MeV/u $^{129}Xe + ^{nat}Cu$ reaction, corrected and projected charged-particle spectrum showing identification of all elements up to the projectile (Z = 54).

Fig. 15 For the 50-MeV/u $^{129}Xe + ^{nat}Cu$ reaction, the density plot of ΔE (5 mm) vs E(plastic) shows the isotopic resolution for hydrogen, helium and lithium isotopes.

Fig. 16 For 2-, 3- and 4-fold events, the total charge detected in the array is plotted for the 40-MeV/u $^{139}La + ^{12}C$, ^{27}Al, ^{51}V, & ^{nat}Cu reactions.

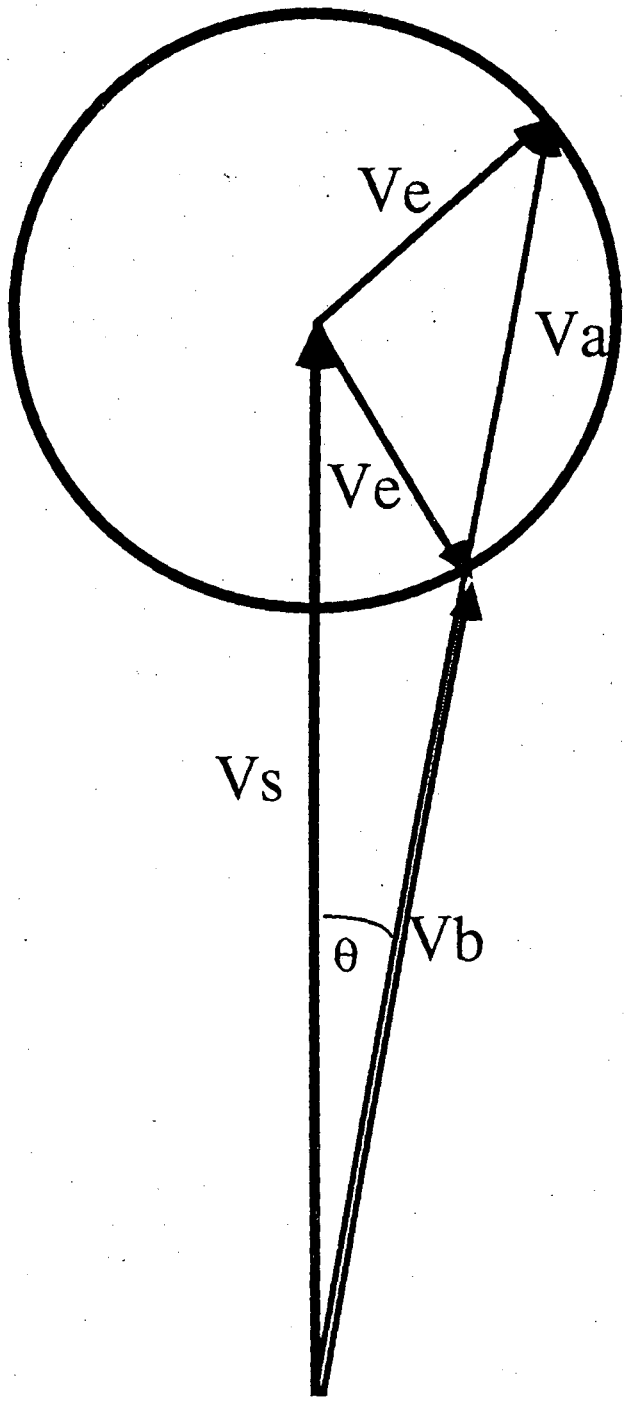

XBL 914-805

Fig. 1

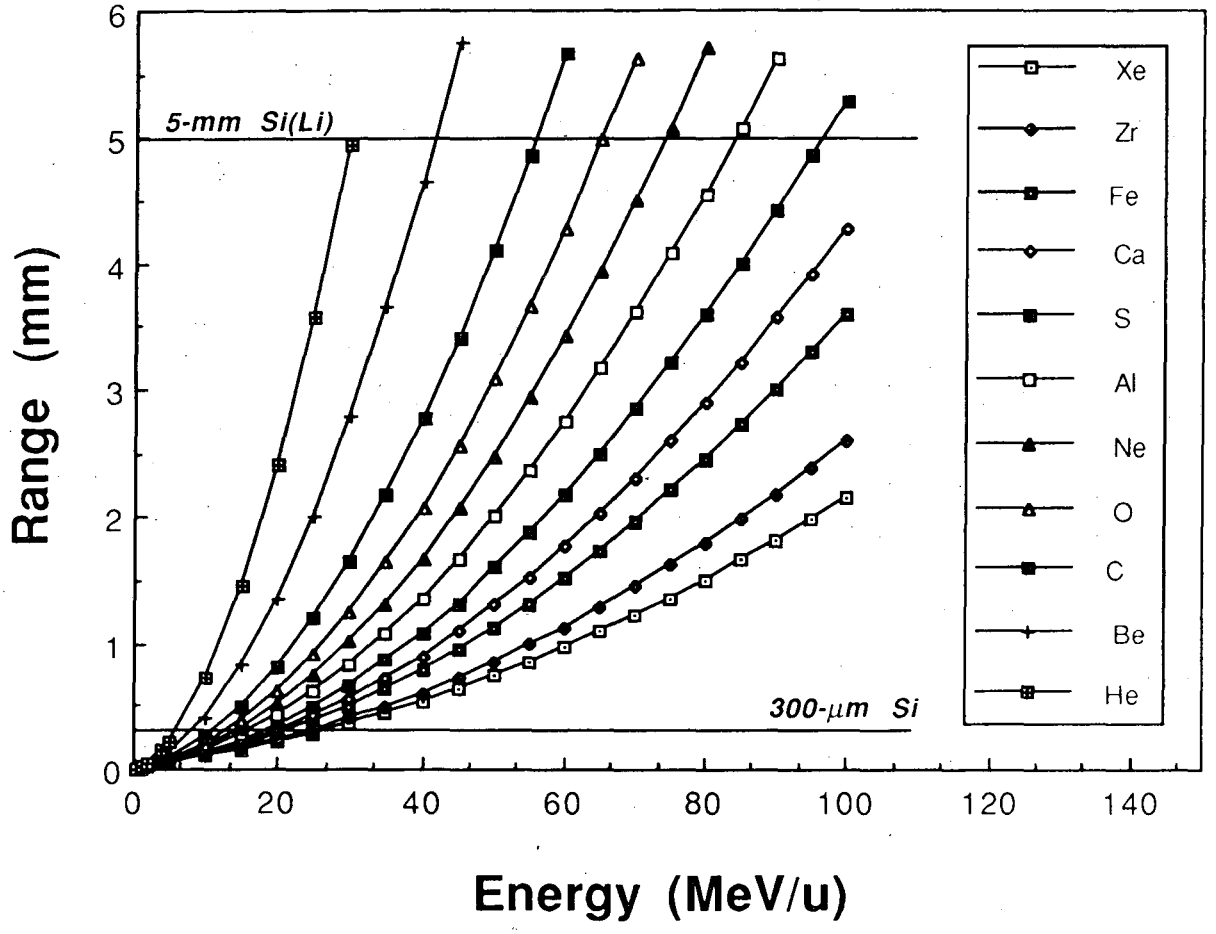

XBL 916-1336

Fig. 2

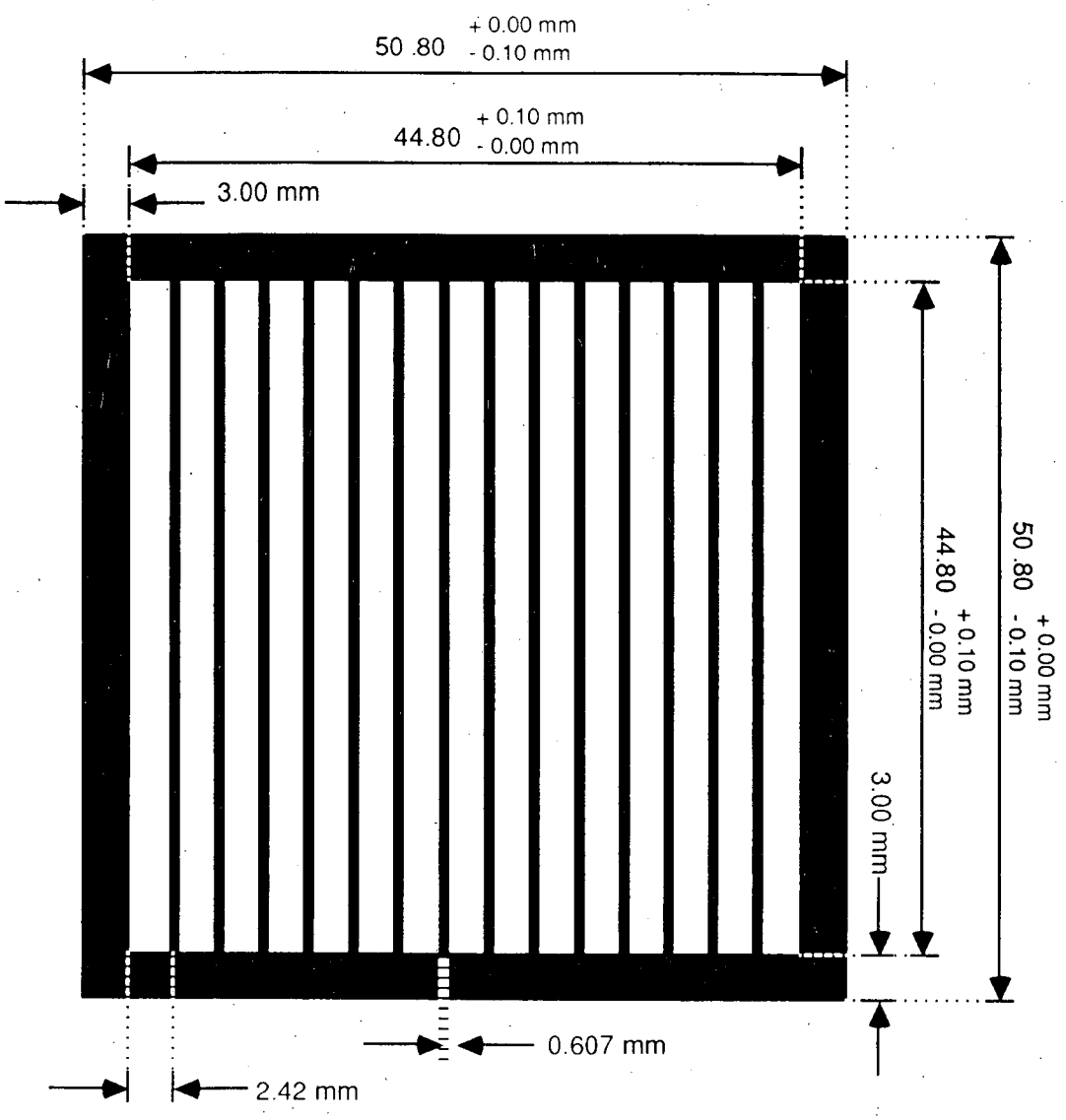
50 .80 + 0.00 mm - 0.10 mm
44.80 + 0.10 mm - 0.00 mm
3.00 mm
50 .80 + 0.00 mm - 0.10 mm
44.80 + 0.10 mm - 0.00 mm
3.00 mm
0.607 mm
2.42 mm
XBL 916-1335

Fig. 3

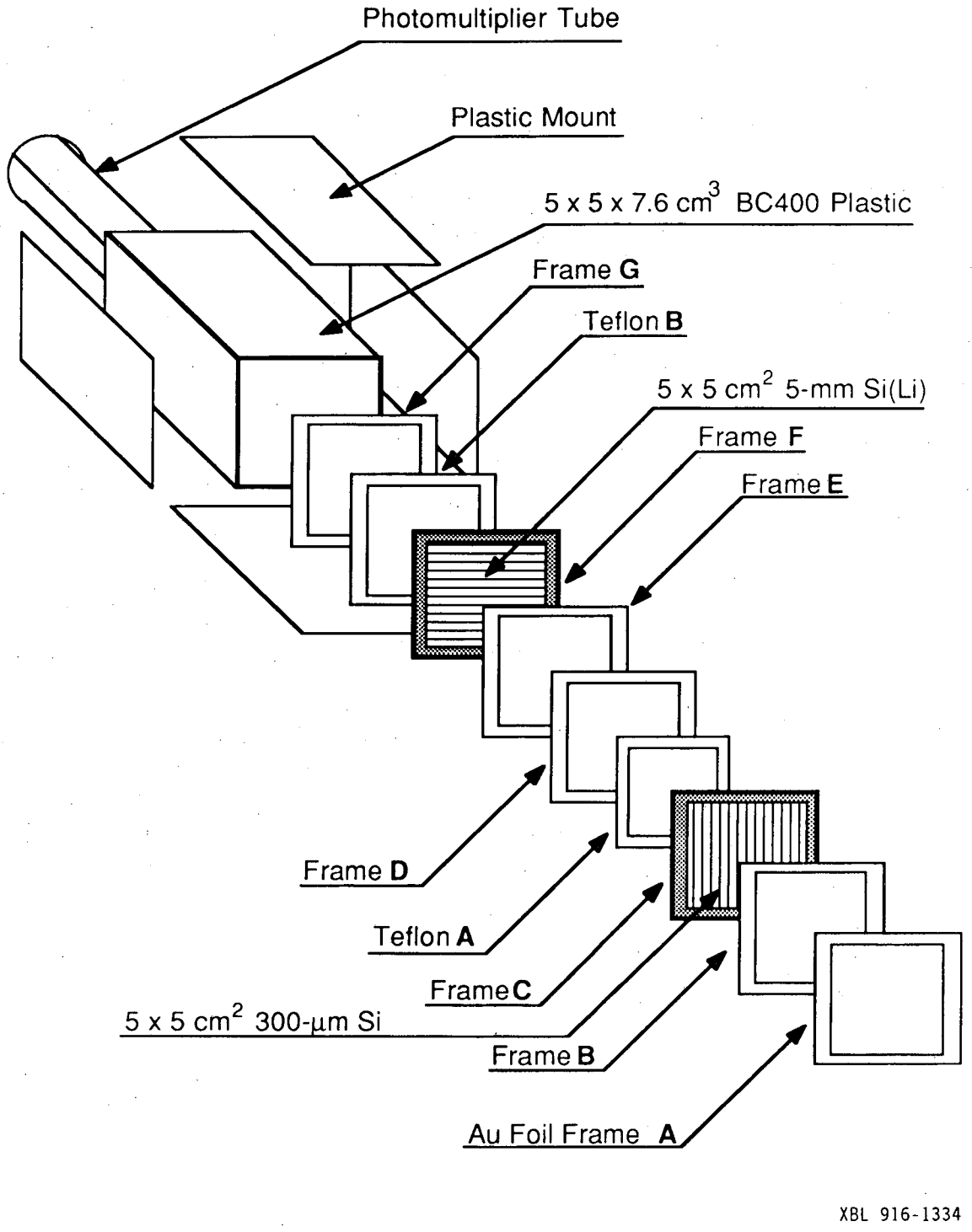
Photomultiplier Tube
Plastic Mount
5 x 5 x 7.6 cm3 BC400 Plastic
Frame G
Teflon B
5 x 5 cm2 5-mm Si(Li)
Frame F
Frame E
Frame D
Teflon A
Frame C
5 x 5 cm2 300-μm Si
Frame B
Au Foil Frame A
XBL 916-1334

Fig. 4

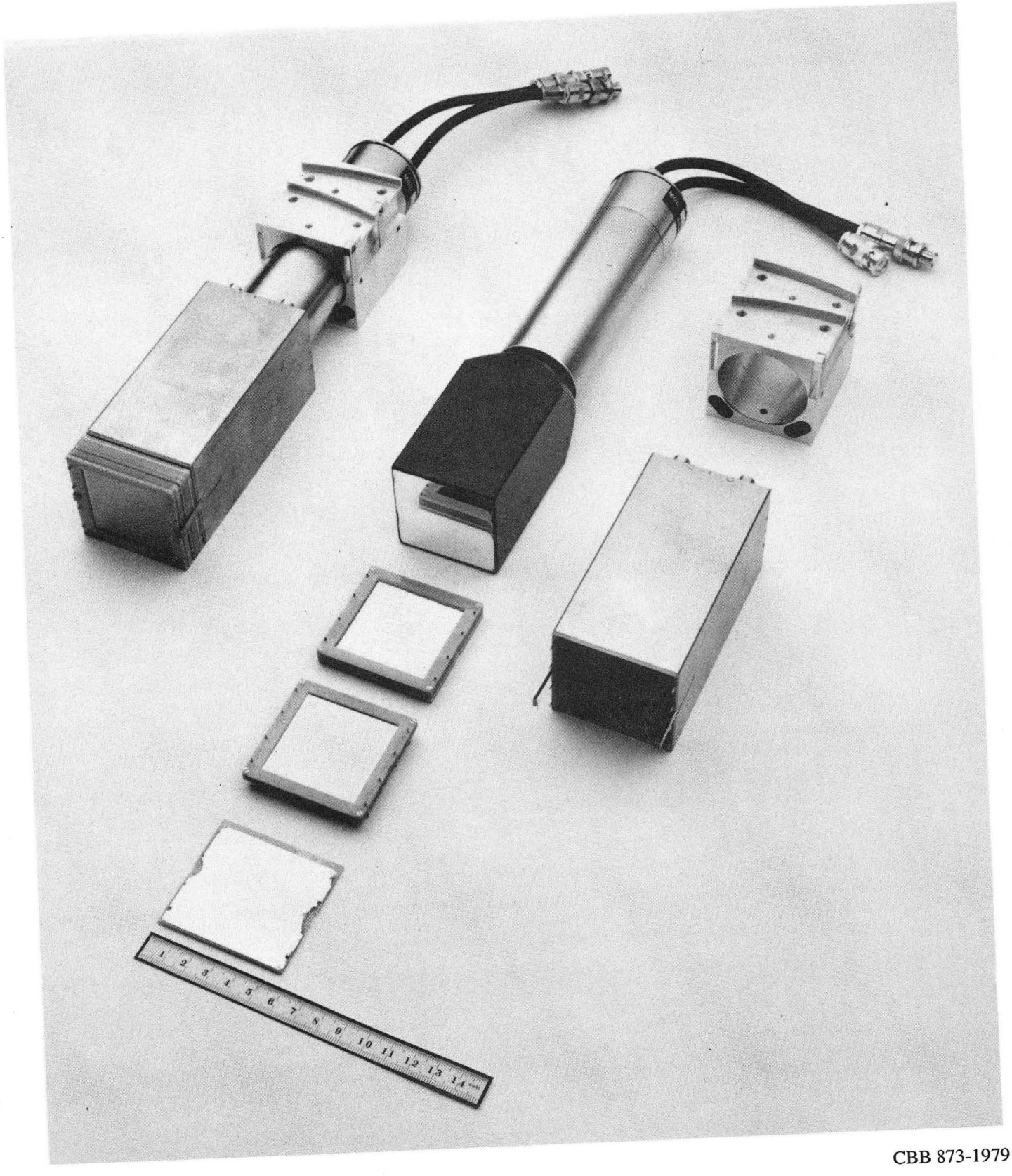

CBB 873-1979

Fig. 5

a)

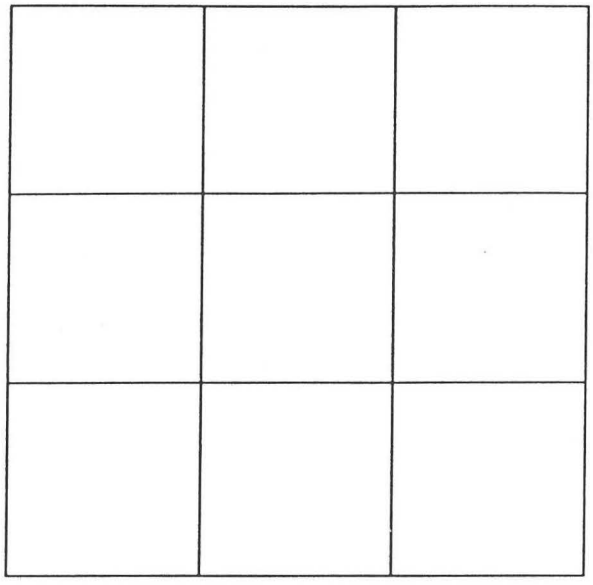

b)

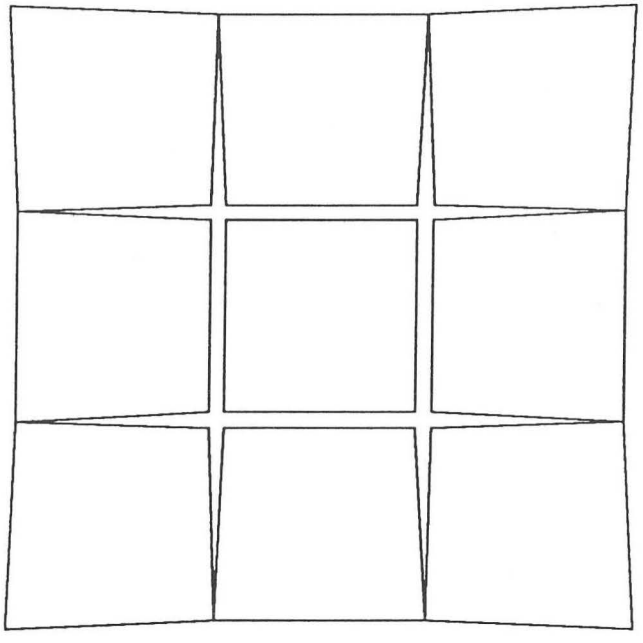

XBL 916-1333

Fig. 6

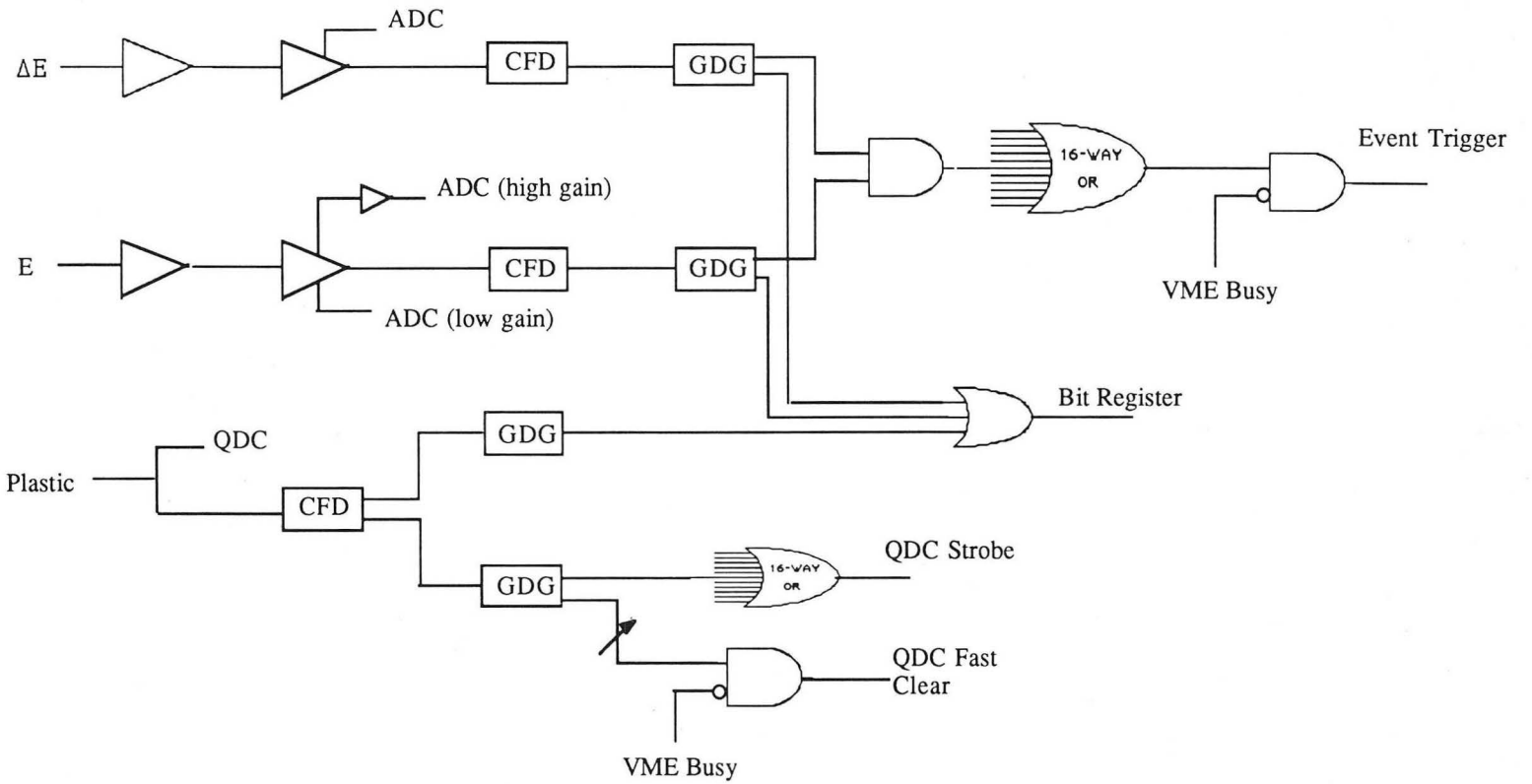

Legend

ADC: Analog-to-Digital Converter
CFD: Constant Fraction Discriminator
GDG: Gate and Delay Generator
QDC: Charge-to-Digital Converter
TDC: Time-to-Digital Converter

Fig. 7

XBL 916-1332

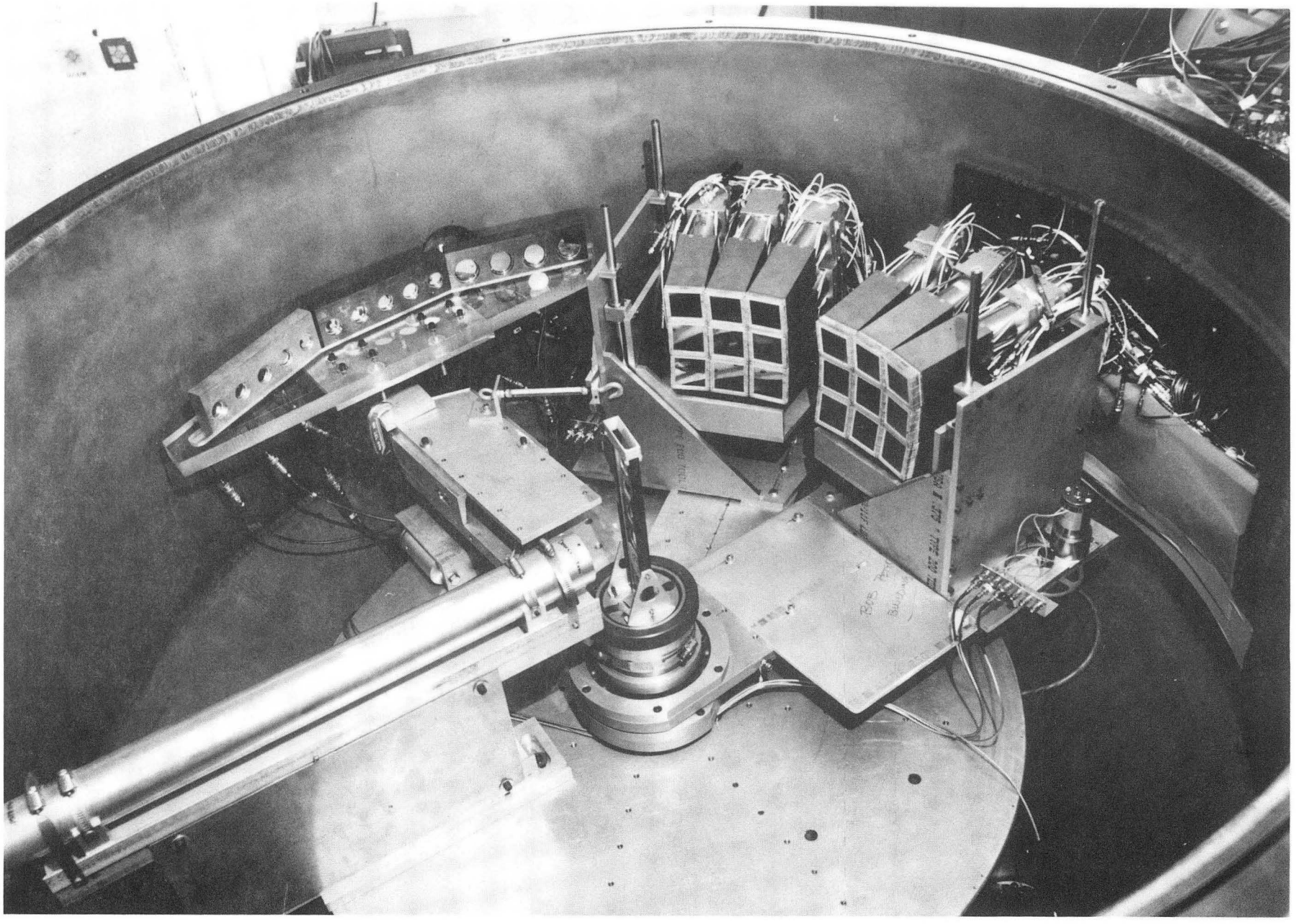

CBB 904-3054

Fig. 8

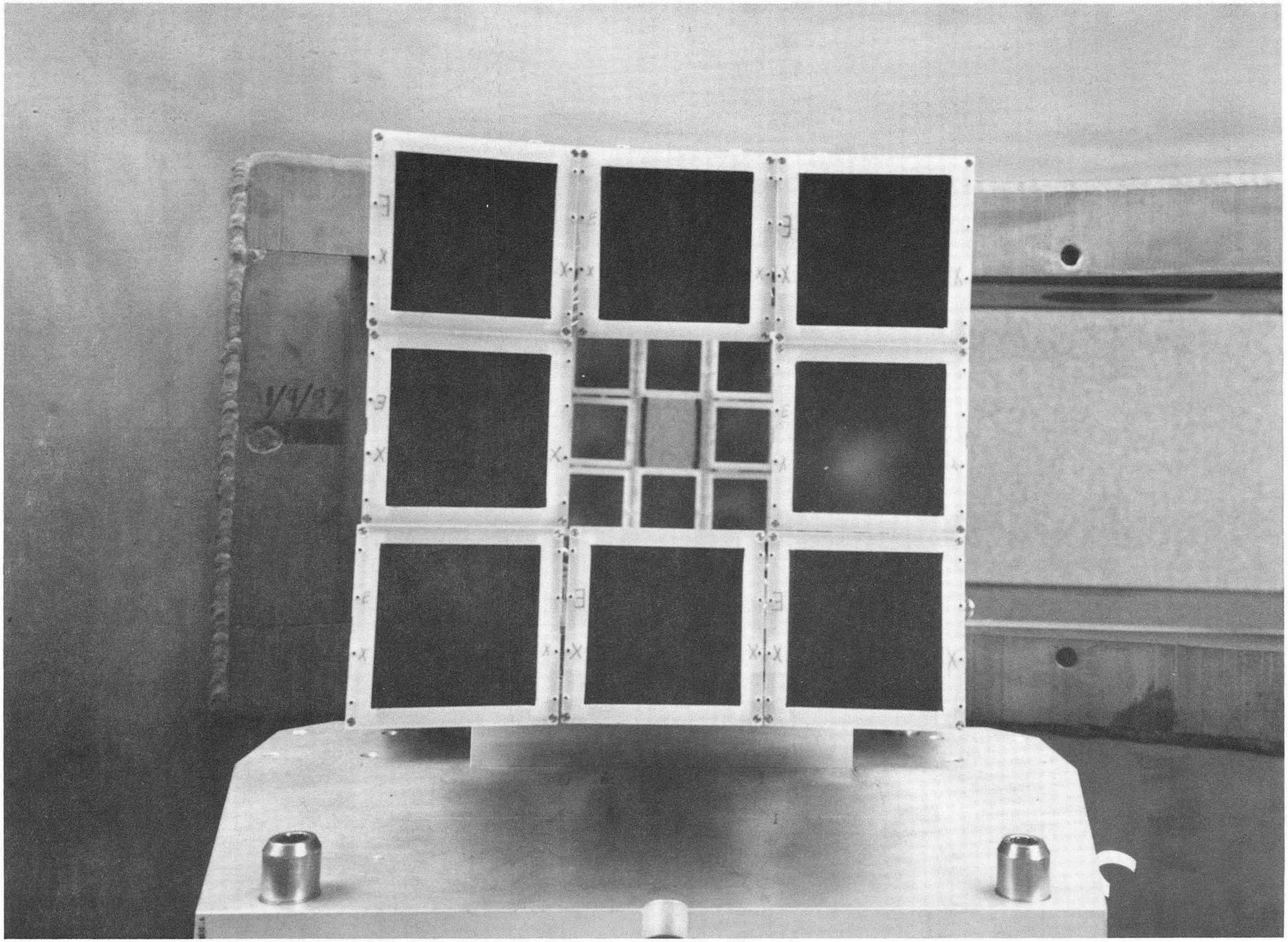

CBB 889-9136

Fig. 9

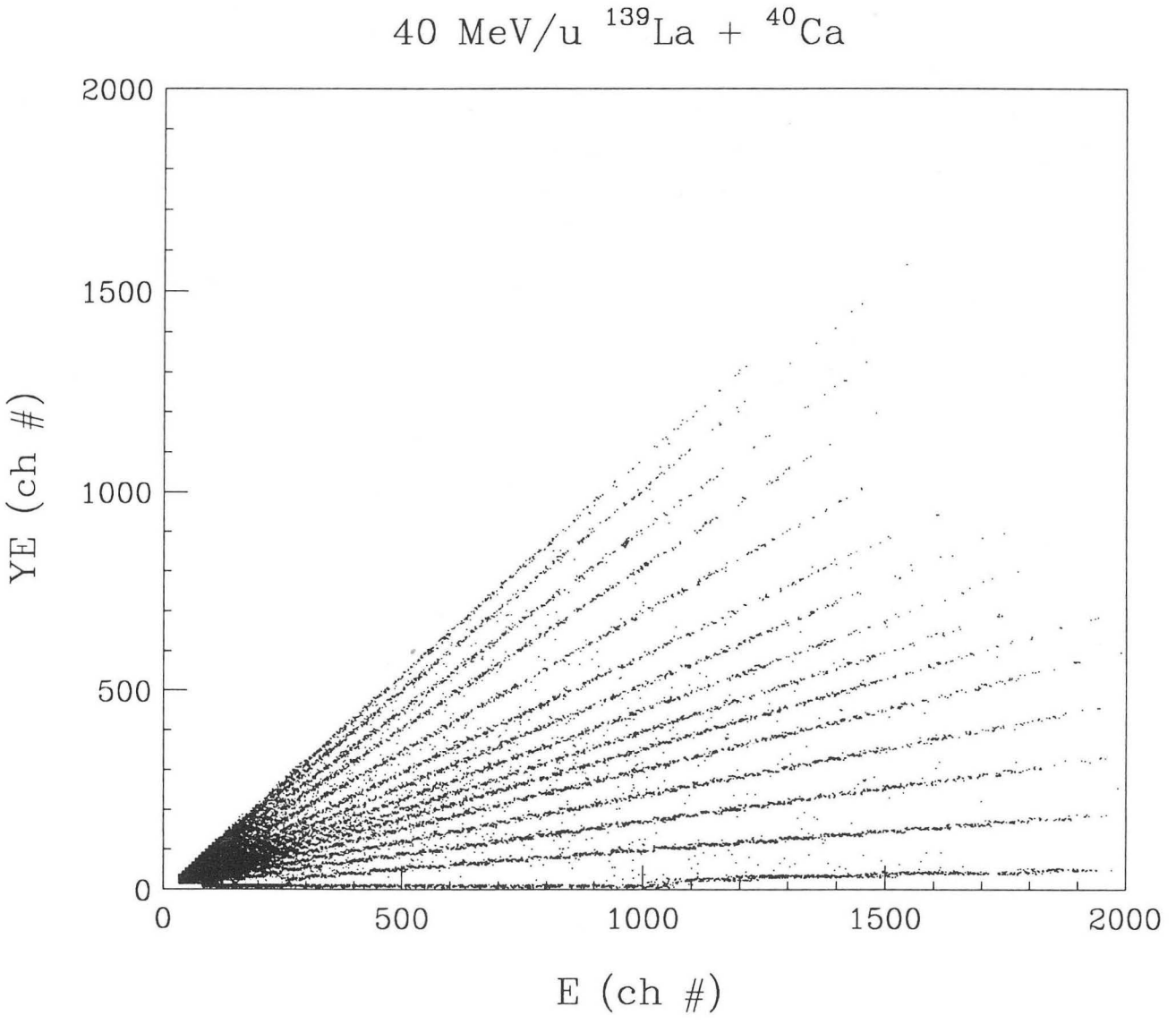
40 MeV/u ^{139}La + ^{40}Ca
2000
1500
1000
500
0
YE (ch #)
0
500
1000
1500
2000
E (ch #)
XBL 916-1331

Fig. 10

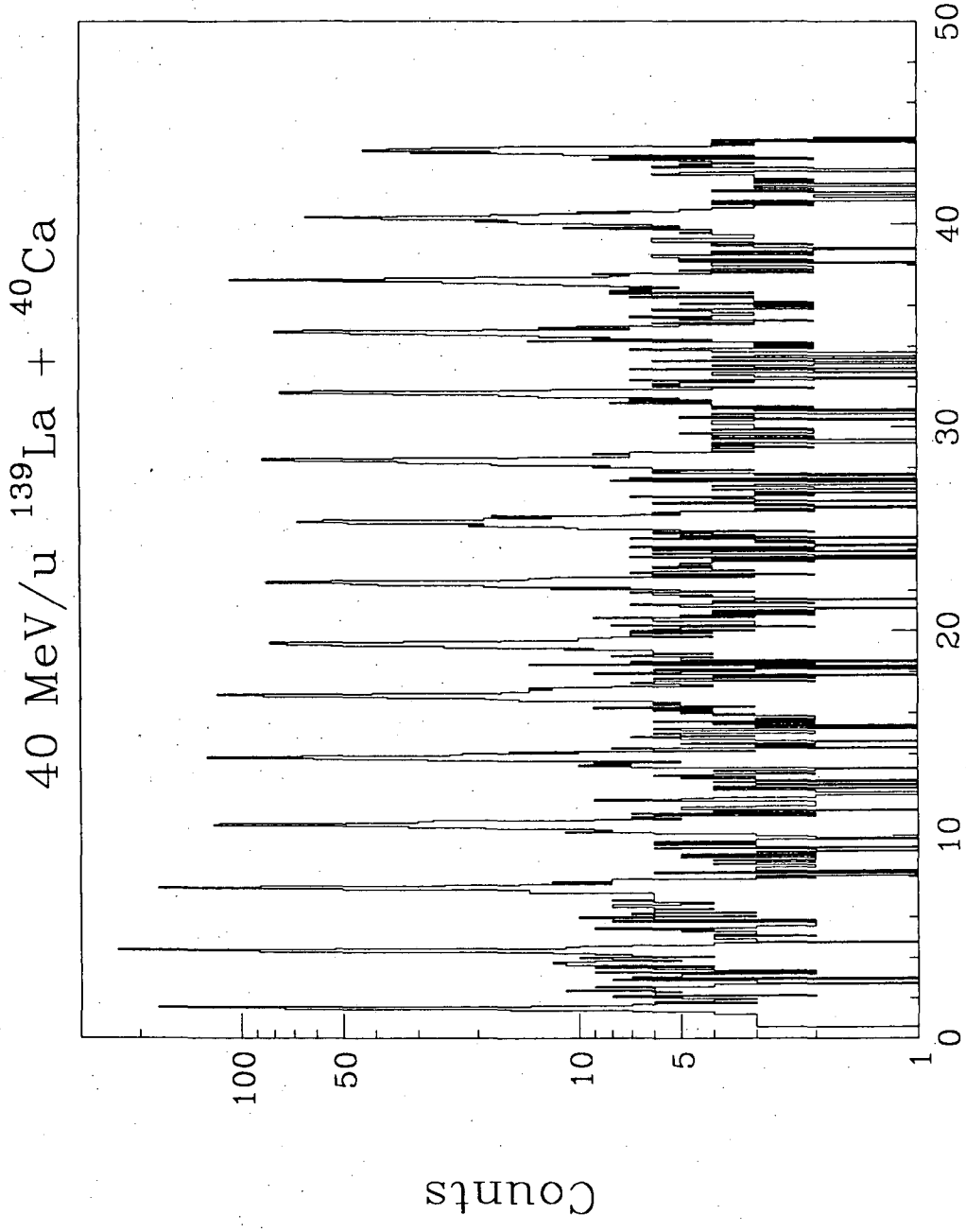

XBL 916-1330

Fig. 11

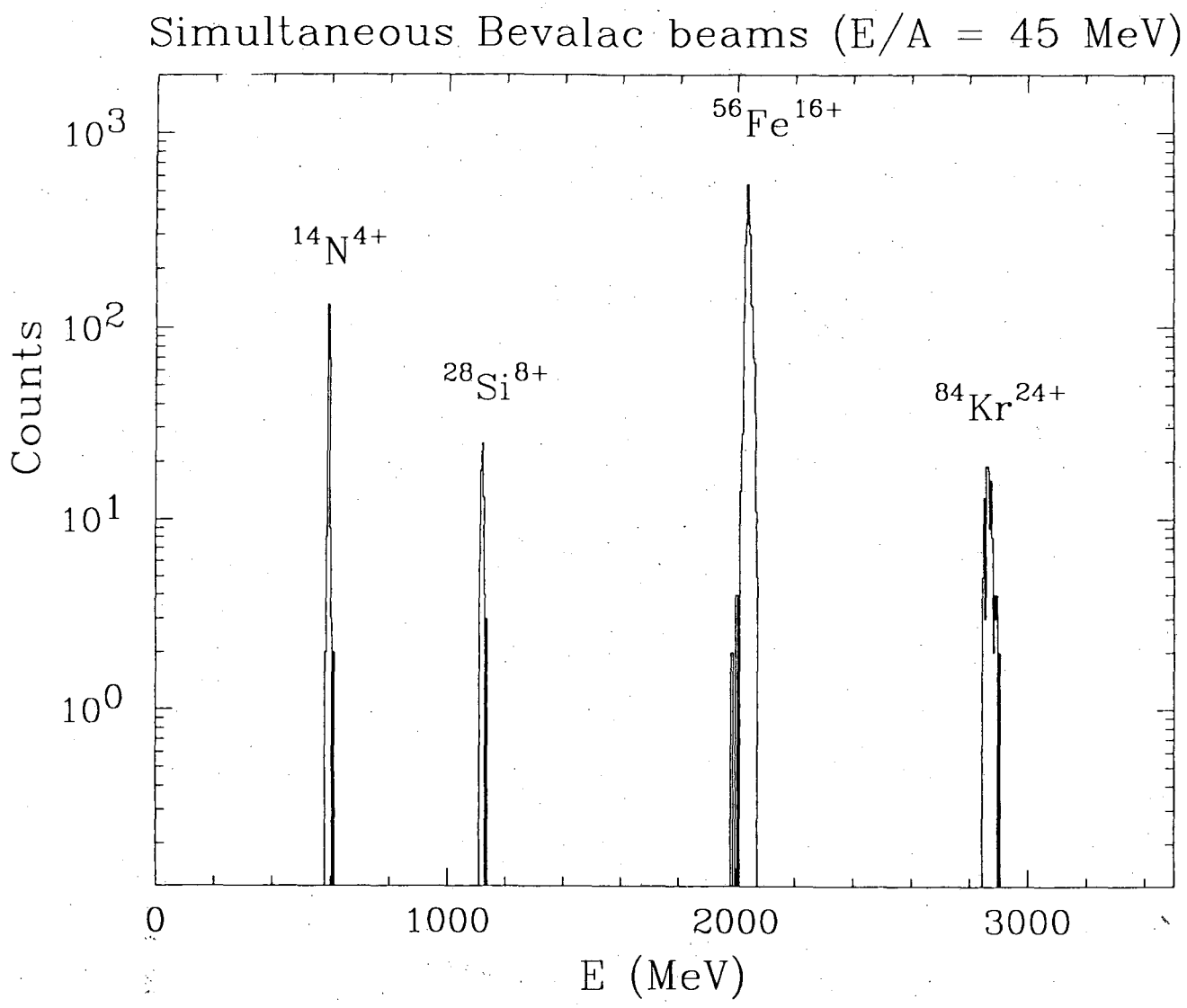
Simultaneous Bevalac beams (E/A = 45 MeV)
Counts
10^3
10^2
10^1
10^0
$^{14}N^{4+}$
$^{28}Si^{8+}$
$^{56}Fe^{16+}$
$^{84}Kr^{24+}$
0
1000
2000
3000
E (MeV)
XBL 916-1325

Fig. 12

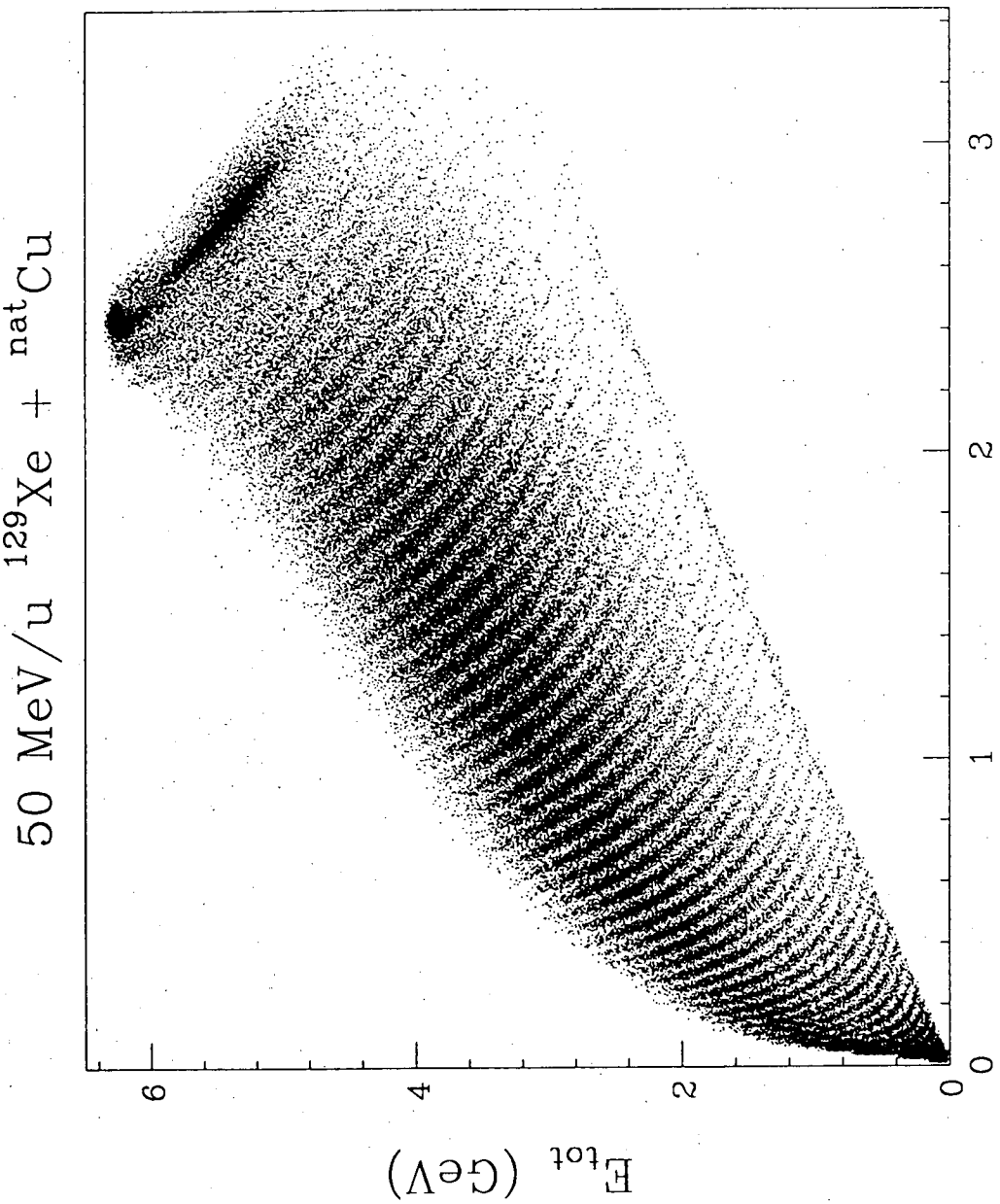

XBL 916-1329

Fig. 13

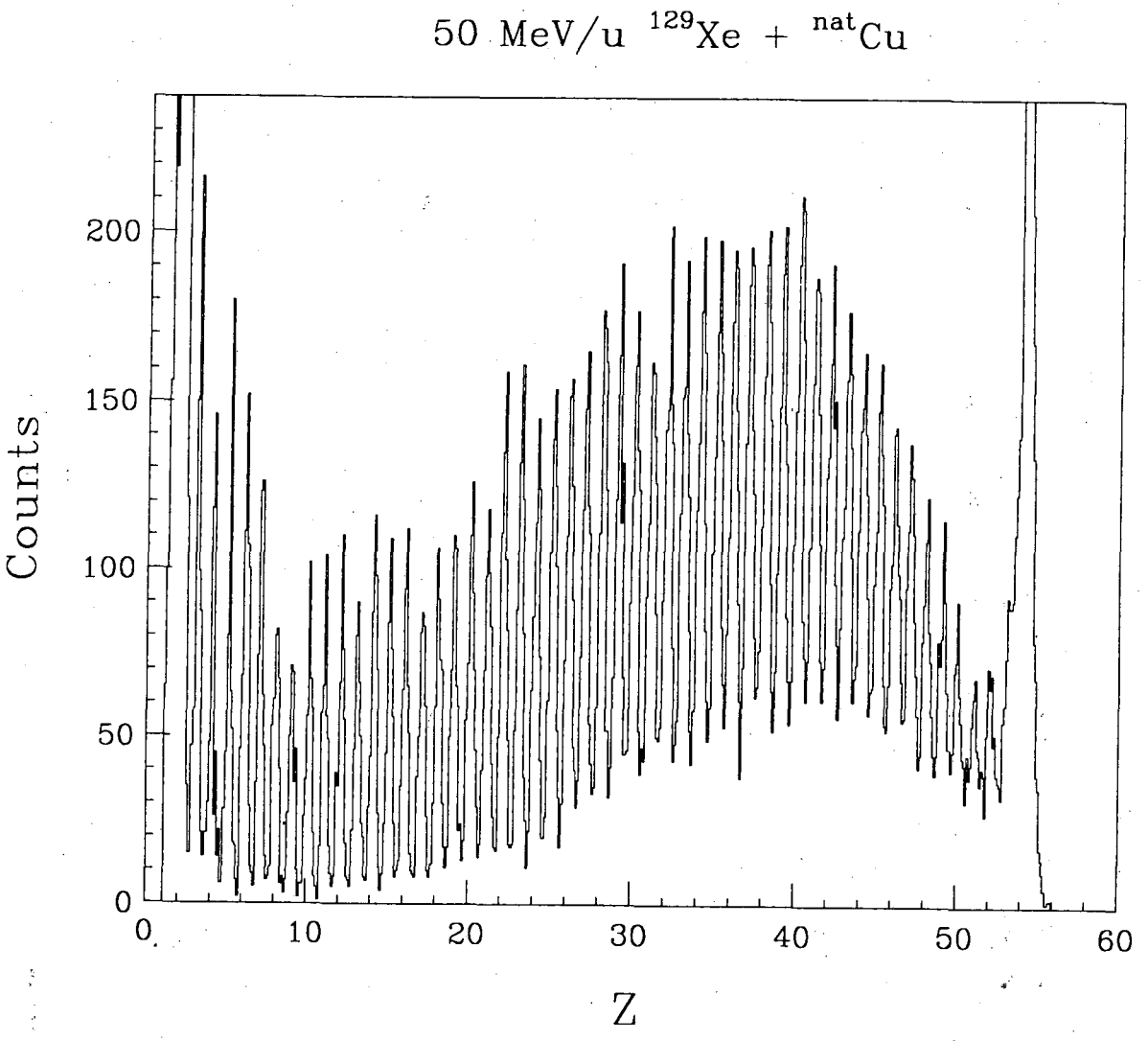
50 MeV/u ^{129}Xe + ^{nat}Cu
Counts
Z
0
50
100
150
200
0
10
20
30
40
50
60
XBL 916-1328

Fig. 14

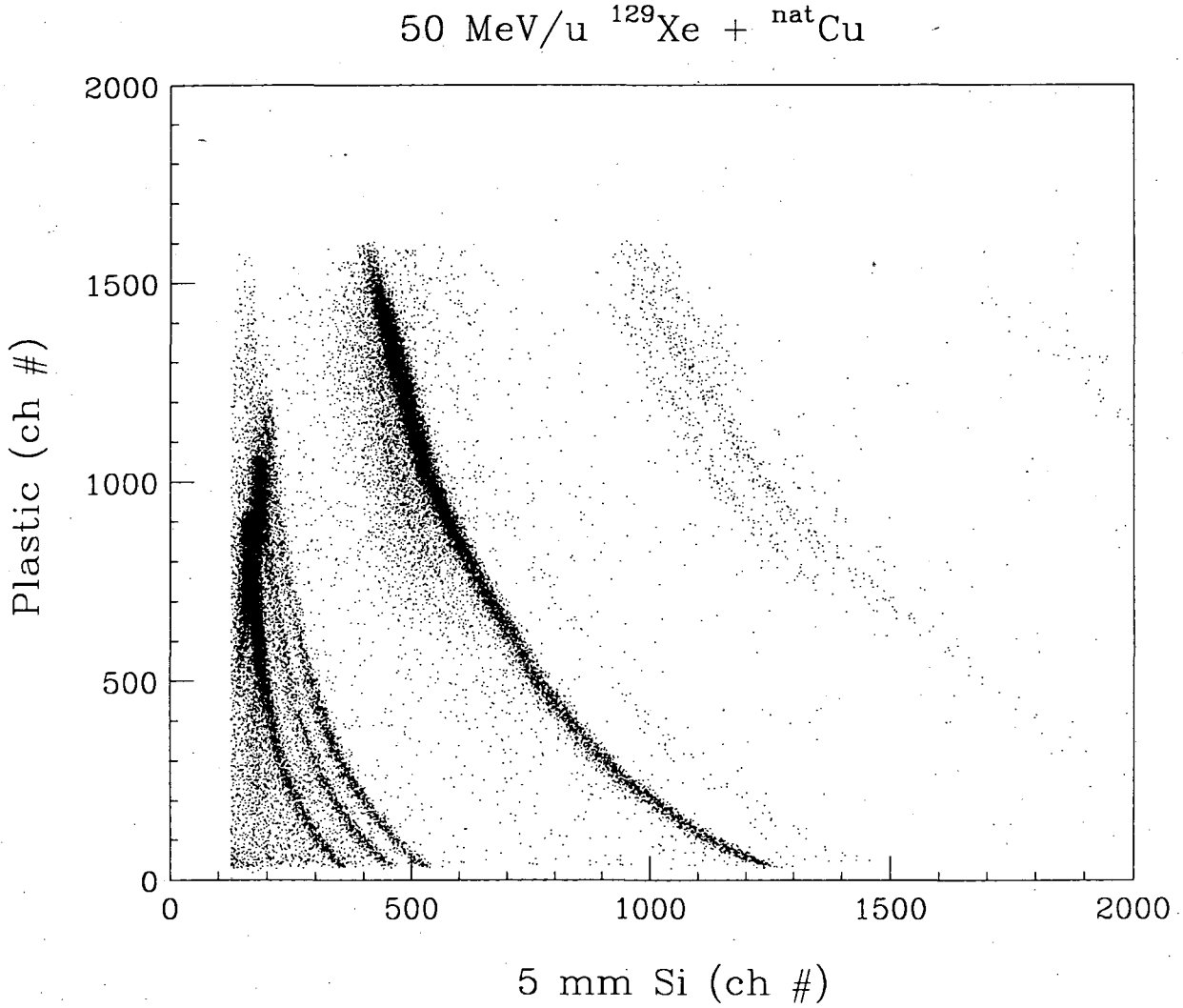
50 MeV/u ^{129}Xe + ^{nat}Cu
Plastic (ch #)
5 mm Si (ch #)
0
500
1000
1500
2000
XBL 916-1327

Fig. 15

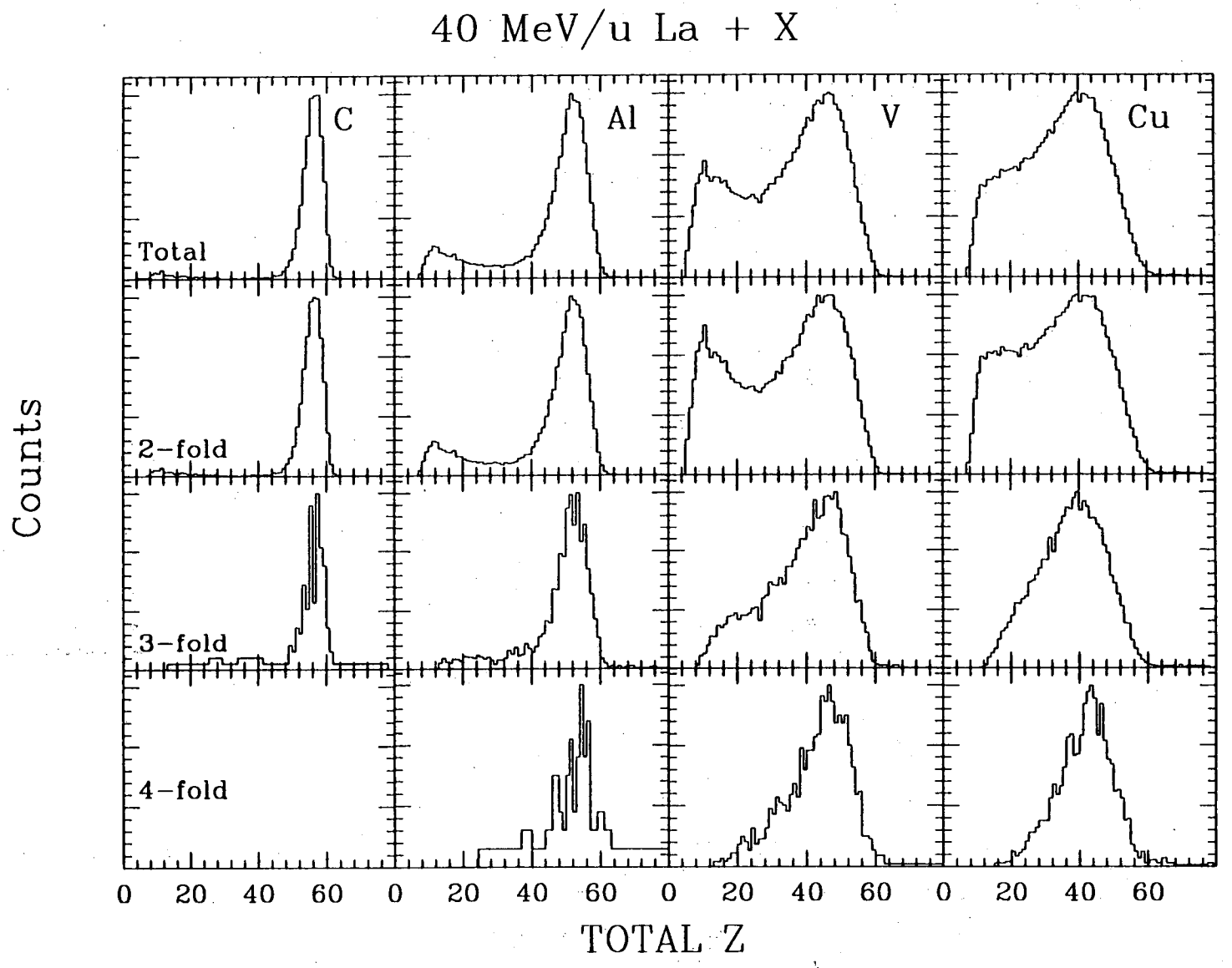
40 MeV/u La + X
C
Al
V
Cu
Total
2-fold
3-fold
4-fold
Counts
0
20
40
60
TOTAL Z
XBL 916-1326

Fig. 16

LAWRENCE BERKELEY LABORATORY
UNIVERSITY OF CALIFORNIA
INFORMATION RESOURCES DEPARTMENT
BERKELEY, CALIFORNIA 94720